

See discussions, stats, and author profiles for this publication at: <https://www.researchgate.net/publication/274011611>

Phase Transformation Fabrication of a Cu₂S Nanoplate as an Efficient Catalyst for Water Oxidation with Glycine

ARTICLE in INORGANIC CHEMISTRY · MARCH 2015

Impact Factor: 4.76 · DOI: 10.1021/ic502920r · Source: PubMed

CITATIONS

2

READS

78

8 AUTHORS, INCLUDING:



Panpan Zhou

Lanzhou University

40 PUBLICATIONS 181 CITATIONS

[SEE PROFILE](#)



Fengjuan Chen

Lanzhou University

38 PUBLICATIONS 661 CITATIONS

[SEE PROFILE](#)



Hongyan Liu

Lanzhou University

25 PUBLICATIONS 546 CITATIONS

[SEE PROFILE](#)



Pinxian Xi

Lanzhou University

43 PUBLICATIONS 916 CITATIONS

[SEE PROFILE](#)

Phase Transformation Fabrication of a Cu₂S Nanoplate as an Efficient Catalyst for Water Oxidation with Glycine

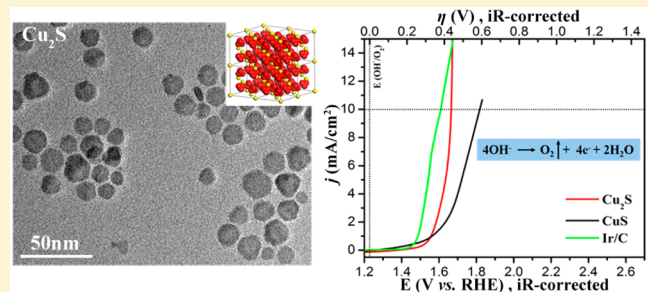
Li An,[†] Panpan Zhou,[†] Jie Yin,[†] He Liu,[†] Fengjuan Chen,[†] Hongyan Liu,[†] Yaping Du,[‡] and Pinxian Xi*,[†]

[†]Key Laboratory of Nonferrous Metal Chemistry and Resources Utilization of Gansu Province, State Key Laboratory of Applied Organic Chemistry and College of Chemistry and Chemical Engineering, and The Research Center of Biomedical Nanotechnology, Lanzhou University, Lanzhou 730000, P. R. China

[‡]Frontier Institute of Chemistry, Frontier Institute of Science and Technology Jointly with College of Science, State Key Laboratory for Mechanical Behavior of Materials, Xi'an Jiaotong University, Xi'an 710049, P. R. China

Supporting Information

ABSTRACT: The synthesis of semiconducting nanoplates (NPs) with defined crystal phase is of particular interest, especially their intriguing properties related to the size, shape, and crystal phase. Herein, a liquid-state transformation process from hexagonal-phase CuS NPs is employed to fabricate the cubic-phase Cu₂S NPs. The CuS NPs were converted into Cu₂S NPs but maintained the morphology. The Cu₂S NPs exhibit better oxygen evolution reaction (OER) activity than CuS NPs. Furthermore, the OER activity of Cu₂S NPs can be improved by the addition of a glycine (Gly) solution. The Cu₂S NPs with Gly in a phosphate buffer solution exhibit excellent OER activity and durability, which approaches that of the best known commercial Ir/C (20%) nanocatalyst. In this work, a good strategy for fabricating a noble-metal-free OER catalyst has been proposed, which could provide insight into developing new water oxidation catalysts with high activity.



INTRODUCTION

Oxygen evolution reaction (OER) in producing O₂ via electrochemical oxidation of water is of great importance in the processes of energy conversion and storage, metal–air batteries, and water splitting.^{1–3} In the water-splitting process, the OER efficiency is considered to be the major bottleneck because the transfer rate of the four electrons involved is slow⁴ and the activation energy barrier of O–O bond formation is high.^{5–7} Generally, OER at the anode is a slow reaction, which requires an overpotential in substantial excess of its thermodynamic potential [1.23 V vs reversible hydrogen electrode (RHE) at standard temperature and pressure] to deliver an acceptable current density.⁸ One of the challenges for OER is how to develop an efficient catalyst applicable for water oxidation with a low overpotential, good stability, and high turnover rates.⁹ An efficient OER catalyst has the ability to promote the proton-coupled electron transfer (PCET) reaction in evolving O₂ under low overpotential.¹⁰ Although Ir- or Ru-based catalysts are the most active materials for OER, their high costs and scarcity greatly restrict their industrial application.¹¹ Many OER catalysts were developed based on 3d metal (e.g., Fe, Cu, Co, Ni, and Mn), for instance, single- and mixed-metal oxides (hydroxides),^{12,13} chalcogenides,¹⁴ phosphates,¹⁵ borides,¹⁶ perovskites,¹⁷ and molecular catalysts,¹⁸ for they have the advantages of low costs, high chemical stability, and electrocatalytic ability. However, the sluggish kinetics of OER limits the O₂ yields of water splitting,¹⁹ causing the requirement

of considerable overpotential. Thereby, designing highly active OER catalysts to realize more energy efficiency of the whole water-splitting reaction is crucial. As an earth-abundant and biorelevant metal, Cu is rarely used in water oxidation. Recently, Mayer et al. had reported that Cu^{II} with 2,2'-bipyridine can serve as a catalyst for water oxidation.²⁰ Chen and Meyer had presented the CuSO₄ in Na₂CO₃ solution (1 M, pH = 10.8)²¹ and the Cu^{II} complex and triglycylglycine macrocyclic ligand (TGG⁴⁺) with Cu^{II}²² which are effective in OER electrocatalysis. De Lacey et al. had used the enzyme laccase, which contains Cu as a bioelectrocatalyst for OER.²³ These studies using the Cu complex as a catalyst for OER inspired us to investigate the OER catalytic performance of the nanomaterials like copper sulfide nanocrystals (NCs).

For the copper sulfide system, two main solid phases exist: CuS (covellite) and Cu₂S (chalcocite). They are believed to be p-type semiconducting materials for the Cu vacancies within the lattice.²⁴ Cu₂S is an important component in solar cells, cold cathodes, and nanoscale switches.²⁵ However, the structures of Cu_{2-x}S phases are still not clear because the positions of the Cu and S atoms have not been well-defined. Because of this special status, CuS is the ideal candidate starting crystal structural model for precise control synthesis of other compositions. Meanwhile, the use of a ligand with metal ions to

Received: December 7, 2014

enhance the catalytic properties has been reported like tetraGly peptide with Cu^{II} and glycine (Gly) with Ni^{II}.^{22,26} Thus, in this work, a facile strategy to achieve phase transformation from CuS to Cu₂S nanoplates (NPs) through a reduction process by keeping their original morphology was reported, and their OER performance was examined. Moreover, the effects of Gly, which could enhance the OER performance of Cu₂S NPs, were also explored.

RESULTS AND DISCUSSION

A phase transformation process was developed to synthesize monodisperse Cu₂S NPs. First, monodisperse CuS NPs were formed after the injection of 1-octadecene (ODE)-S into CuCl in hexadecylamine, which is used as (001) face-selective agents and capping ligands.²⁷ Transmission electron microscopy (TEM) analysis suggests that the as-synthesized CuS NPs are monodisperse with dimensions of 11.0 nm × 3.2 nm (diameter × thickness) with an aspect ratio (AR = diameter/thickness) of 3.43 (Figure 1a). In Figure 1b, high-resolution TEM (HRTEM) indicates that the interplane distances between

the lattice fringes are 0.19 and 0.26 nm, corresponding to the (110) and (006) planes of CuS NPs, respectively. X-ray diffraction (XRD) was used to characterize the crystal structure of the product obtained. The diffraction patterns confirmed hexagonal-phase CuS NPs (JCPDS 1-1281, *P*6₃/mmc; Figure 1e), agreeing with the selected-area diffraction (SAED) pattern (inset of Figure 1b). Monodisperse Cu₂S NPs were fabricated by reduction of the 11.0 nm CuS NPs (AR = 3.43) in ODE with oleylamine (OAm) at 220 °C for 1 h. TEM analysis shows Cu₂S NPs with dimensions of 15.9 nm × 4.6 nm with an AR of 3.45 (Figure 1c). The HRTEM image of Cu₂S NPs (Figure 1d) indicates that the interplane distances between the lattice fringes are 0.20 and 0.28 nm, corresponding to the (200) and (220) planes of Cu₂S NPs, respectively. The SAED pattern of the Cu₂S NPs (inset of Figure 1d) also reveals that the diffraction rings correspond to the specific crystalline planes of Cu₂S, indicating the polycrystalline structures of the products. After the phase transformation, all of the diffraction peaks correspond to the reflection of the cubic phase of Cu₂S NPs (chalcopyrite, JCPDS 84-1770, *Fm*3̄*m*; Figure 1e). This illustrates that the products are single-phase Cu₂S with high purity. Furthermore, the Cu₂S NPs obtained are well-crystallized, as can be seen from the intense and sharp diffraction peaks in Figure 1e. The near-IR absorption peak of CuS NPs at 1200 nm is red-shifted to 1400 nm through the transformation fabrication process (Figure S1 in the Supporting Information, SI), further confirming the formation of Cu₂S NPs.²⁸ To investigate the conduction band (CB) and valence band (VB) levels of Cu₂S NPs, cyclic voltammetry (CV) analysis was performed with an Ag/AgCl reference electrode. Also, the ferrocene/ferrocenium redox couple (Fc/Fc⁺, -4.8 eV) was used as the reference material for all CV measurements. The oxidation potential onset of ferrocene, as marked by the vertical dotted line (Figure S2 in the SI), is estimated to be 0.35 V (vs Ag/AgCl). Using ferrocene as the reference material, the CB and VB energy levels of the CuS and Cu₂S NPs can be calculated by the following equation:²⁹

$$E_{\text{CB/VB}} = -[(E_{\text{red/ox}} - E_{\text{ferrocene}}) + 4.8] \text{ eV}$$

The calculated CB, VB, and electrochemical band gaps of CuS and Cu₂S NPs (Table 1) are similar to the reported band gaps that are suitable for OER applications.³⁰

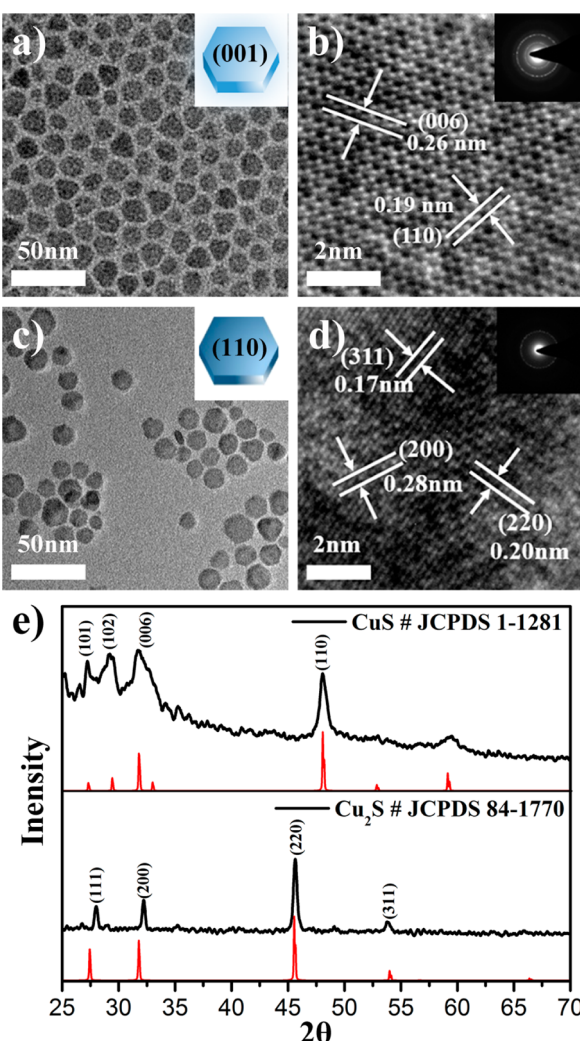


Figure 1. (a) TEM and (b) HRTEM images of 11.0 nm (AR = 3.43) CuS NPs. The inset of part b is the SAED image of CuS NPs. (c) TEM and (d) HRTEM images of 15.9 nm (AR = 3.45) Cu₂S NPs. The inset of part d is the SAED image of Cu₂S NPs. (e) XRD patterns of the 11.0 nm CuS NPs and 15.9 nm Cu₂S NPs.

Table 1. Comparison of the CB and VB Energy Levels as Well as the Electrochemical Band Gaps of CuS NPs and Cu₂S NPs

sample	<i>E</i> _{red} [V]	<i>E</i> _{ox} [V]	<i>E</i> _{CB} [eV]	<i>E</i> _{VB} [eV]	<i>E</i> _g [eV]
Cu ₂ S	-0.42	0.79	-4.03	-5.24	1.21
CuS	-0.64	1.29	-3.81	-5.74	1.93

The valence states and purity of these NPs were further characterized by the XPS measurements (Figure 2). All of the binding energies have been calibrated by referencing C 1s (284.6 eV). As shown in Figure 2a, two separate peaks were found at the binding energies of 931.8 and 951.6 eV. They are attributed to Cu 2p_{3/2} and Cu 2p_{1/2}, belonging to Cu²⁺. Additionally, the “shake-up” satellite peaks appear in the higher-binding-energy ranges, indicating the Cu²⁺ valence state.³¹ As observed from Figure 2b, the locations of the binding energy peaks of Cu 2p at 932.2 and 951.9 eV are indicative of the photoelectron states of Cu 2p_{3/2} and Cu 2p_{1/2} of Cu₂S, respectively. For data fitting of the S 2p XPS signal collected on

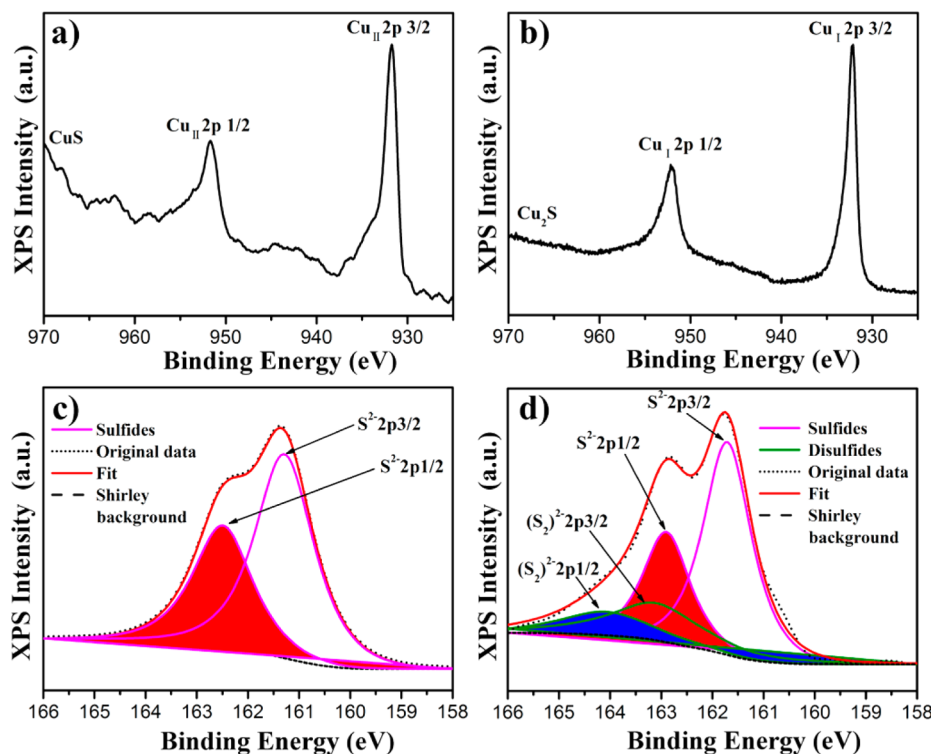


Figure 2. XPS spectra of Cu 2p of (a) CuS and (b) Cu₂S NPs and S 2p of (c) CuS and (d) Cu₂S NPs.

the as-synthesized CuS and Cu₂S NPs, a doublet was used for each S species. Figure 2c shows the S 2p spectrum of the CuS NPs, while no disulfides are observed. In Figure 2d, the S 2p fitting of the Cu₂S peak reveals the presence of two main doublets, which can be ascribed to S²⁻ (purple curves) and (S₂)²⁻ (green curves) at higher binding energy.³² Estimation of the peak area for the two different S surface species suggests that approximately 26.5% of the initial S²⁻ are converted into (S₂)²⁻ (Figure 2d). The binding energies can be obtained by curve fitting the experimental data after nonlinear background subtraction from the spectra of the S 2p lines. The measured binding energies and more detailed information for this phase transformation are summarized in Table S1 in the SI.

To the best of our knowledge, Cu₂S NPs have not been synthesized by using CuS NPs as the starting material with OAm as the reducing agent. Without OAm, we cannot get the Cu₂S NPs, which means that OAm induces the phase transformation of CuS NPs (Figure S3 in the SI). As such, the addition of OAm was crucial to the structural integrity of the NPs. We compared the space-packing structures of covellite CuS and chalcocite Cu₂S NPs (Figure 3a), and their crystal structures are depicted in Figure S4 in the SI to explore the transformation mechanism. The hexagonal phase of CuS consists of S–CuS₃–Cu–CuS₃ layers and van der Waals layers along the *c* axis (Figure 3a). Many structural models have been proposed for Cu₂S NPs because of the complicated atomic arrangement of the Cu cations.³³ In this study, the ideal structure with Cu³⁺ was used as the structural model for Cu₂S NPs (Figure 3a). The S atoms in both the (001) CuS and (110) Cu₂S planes are hexagonal close-packed (Figure 3b), and the side lengths of the unit parallelograms of (001) of CuS (2.261 Å) and (111) of Cu₂S (2.333 Å) are very close. The significant difference between these CuS and Cu₂S structures is that more Cu cations have been inserted into the interstices of the S sites in Cu₂S NPs, in which there are two hexagonal close-

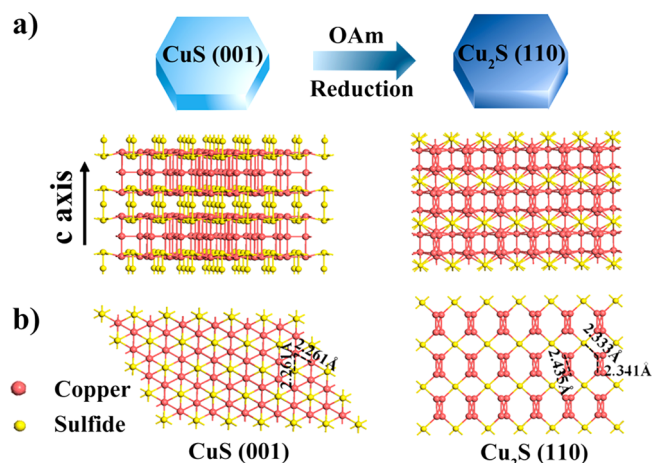


Figure 3. (a) Structural models of covellite CuS NPs and chalcocite Cu₂S NPs. Cu and S atomic arrangements viewed along the *c* axis direction of CuS NPs and Cu₂S NPs. (b) Side views of the (001) surface of CuS NPs and (110) surface of Cu₂S NPs.

packed Cu layers (Figure 3b). Thus, CuS with low occupancy of Cu cations is a good starting material because more Cu cations can be inserted, which facilitates the formation of Cu₂S NPs. The Cu cations with high mobility and ionic diffusivity at high temperature³⁵ enable the inserted Cu cations to move rapidly and occupy the interstices with lower energies, accompanied by the site regulation of preexisting Cu cations.

To perform the OER test, we deposited CuS and Cu₂S NPs on carbon black (Ketjen EC-600J) via sonication of a mixture of a hexane dispersion of the NPs and a carbon suspension in acetone, followed by washing with ethanol to remove the surfactant.³⁶ These materials were uniformly cast onto a rotating disk electrode (RDE; loading ~0.2 mg/cm²) for recording CV curves at 1600 rpm with a scan rate of 10 mV/s.

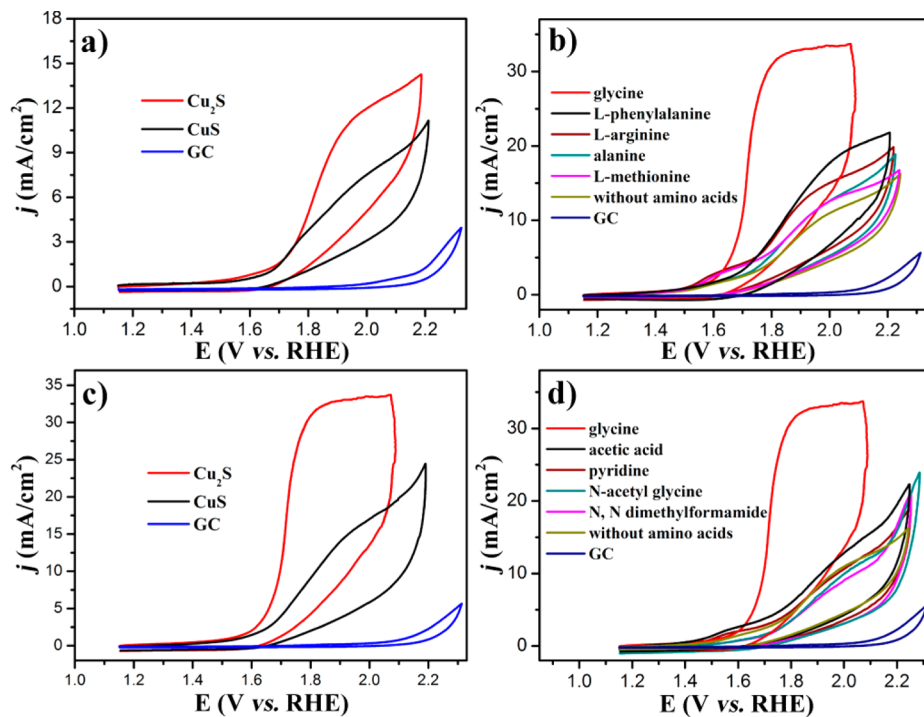
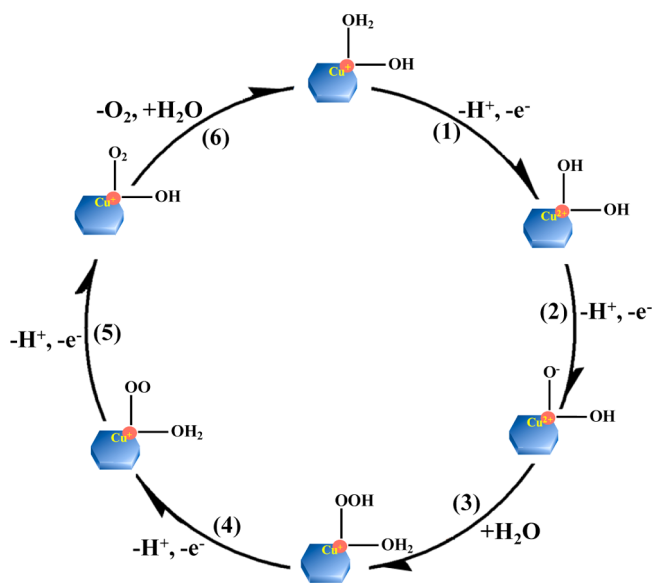


Figure 4. (a) CV curves of Cu₂S, CuS, and GC electrode without amino acids for the OER. (b) CV curves for Cu₂S NPs with amino acids, including Phe, Met, Arg, Ala, and Gly. (c) CV curves of Cu₂S, CuS and GC electrode with Gly for the OER. (d) Current densities for small molecules with different substituents, including pyridine, N-acetyl glycine, N,N-dimethylformamide, and acetic acid. All measurements were carried out by RDE (loading ~ 0.2 mg/cm²) for recording CV curves at a rotation rate of 1600 rpm with a scan rate of 10 mV/s.

We investigated the electrocatalytic OER activity of CuS and Cu₂S NPs in alkaline solutions (phosphate buffer at pH = 13) in a standard three-electrode system. As a control example for referencing, we further measured the commercial Ir/C and Pt/C catalysts (Premetek Co., 20 wt %) with the same ~ 0.2 mg/cm² loading onto the RDE electrode. As shown in Figure 4a, the Cu₂S NPs show a current density of about 11.61 mA/cm² at 1.83 V (vs RHE), which is higher than CuS NPs (8.89 mA/cm²). It could be related to the special property of Cu₂S NPs because it can undergo a conversion of the oxidation state in the OER that is similar to cobalt oxide,³⁷ as shown in Scheme 1. In the OER process, a Cu atom with an oxidation state of 1+ serves as the center, connected by $-OH$ and H₂O ligands. Because H₂O adsorption on the (110) surface is favorable thermodynamically, the OER directly splits H₂O on a Cu⁺ site to produce an adsorbed $-OH$. $-OH$ then loses a proton to form an O atom, so a Cu $-O^-$ group would form after two PCET steps (steps 1 and 2 in Scheme 1). After the nucleophilic attack of a solvent molecule on the Cu $-O^-$ group, a hydroperoxo CuOOH group as well as the O–O bond was yielded (step 3 in Scheme 1). Then a superoxo (step 4 in Scheme 1) and molecular O₂ (step 5 in Scheme 1) would form via two PCET steps. Finally, O₂ is evolved, and the catalyst is recovered when a H₂O molecule connects to the Cu site (step 6 in Scheme 1).

Notably, step 4 in Scheme 1 involves an important deprotonation process. Therefore, how to promote this process is critical to OER. Amino acid in the basic solution has a structure of H₃N⁺–CH₂–COO[–], which enables it to capture a proton, so employing this entity could promote the deprotonation process. Accordingly, amino acids such as L-phenylalanine (Phe), L-methionine (Met), L-arginine (Arg), alanine (Ala), and Gly were used to examine their effects on

Scheme 1. Proposed Reaction Mechanism for Cu₂S NPs in Water Oxidation



OER with Cu₂S NPs as catalysts. Interestingly, there is a significant current density increase of Cu₂S from 11.61 to 31.94 mA/cm² at 1.83 V (vs RHE) with 6 mM Gly in phosphate buffer; while other amino acids such as Phe, Met, Arg, and Ala were added, the CV curves responded less sensitively compared with Gly (Figure 4b and Table 2), showing that the side chain of the amino acids exhibits no significant effect on the activity (the structures of the amino acids can be found in Figure S5 in the SI). Meanwhile, we also examined the effects of Gly, CuS, and GC (Figure 4c), and it can be found that Gly only shows

Table 2. Current Density and Potential Values of Cu₂S in Different Amino Acids

	amino acids					without amino acids
	Gly	Phe	Arg	Ala	Met	
j [mA/cm ²]	31.94	17.39	14.48	13.51	13.17	11.61
potential [V vs RHE]	1.83	1.99	1.96	2.02	1.96	2.01

obvious enhancement to the current density of Cu₂S (Table 3). Moreover, the additives of acetic acid, pyridine, and *N*-

Table 3. Current Density and Potential Values of Cu₂S, CuS, and GC with and without Gly

electrode	Cu ₂ S		CuS		GC	
	j [mA/cm ²]	potential [V]	j [mA/cm ²]	potential [V]	j [mA/cm ²]	potential [V]
with Gly	31.94	1.83	11.53	2.01	2.55	2.21
without Gly	11.61	1.95	8.89	2.01	2.23	2.01

acetylglycine with a secondary amide and an acetyl substituent had been tested, and only a small current density of less than 13.0 mA/cm² was observed (Figure 4d and Table S2 in the SI). The results suggest that the amine of Gly plays a significant role in the catalysis, which may be attributed to its ability to capture a proton. As a result, the deprotonation process of step 4 in

Scheme 1 is accelerated, which is favorable to the subsequent steps. It is also worth mentioning that the amino acids may also have an impact on the material conductivity, electron transfer ability, and electrocatalytic activity.³⁸ The enhanced catalytic activity of Cu₂S NPs with amino acids is in agreement with the previous work, which uses tetraGly peptide to promote water oxidation.²² Enhancement of the current density for the Cu₂S NPs with Gly in water oxidation indicates that only one primary amine is effective.

To optimize the concentration of Gly in the measuring system, CV measurements were performed in a 250 mM phosphate buffer solution (pH = 13) with various concentrations of Gly (Figure 5a). Increasing the Gly concentration resulted in a decline of the current density after an increase in response, and the optimum concentration of Gly was 6 mM (inset of Figure 5a). It can be concluded that the appropriate amount of Gly can enhance the catalytic activity of Cu₂S for OER. Moreover, CV measurements were performed to investigate the contribution of phosphate by varying concentrations of sodium dihydrogen phosphate (Figure 5b). Increasing the sodium dihydrogen phosphate concentration resulted in an increase of the current density, and the concentration of phosphate at 250 mM is considered to be the best measurement condition (inset of Figure 5b). Thus, phosphate is beneficial for OER, most likely because of its ability to accept a proton.³⁹ The activity of Cu₂S for OER in Gly was critically associated with the pH of the solution, as shown in Figure 5c. The anodic peak systematically shifted

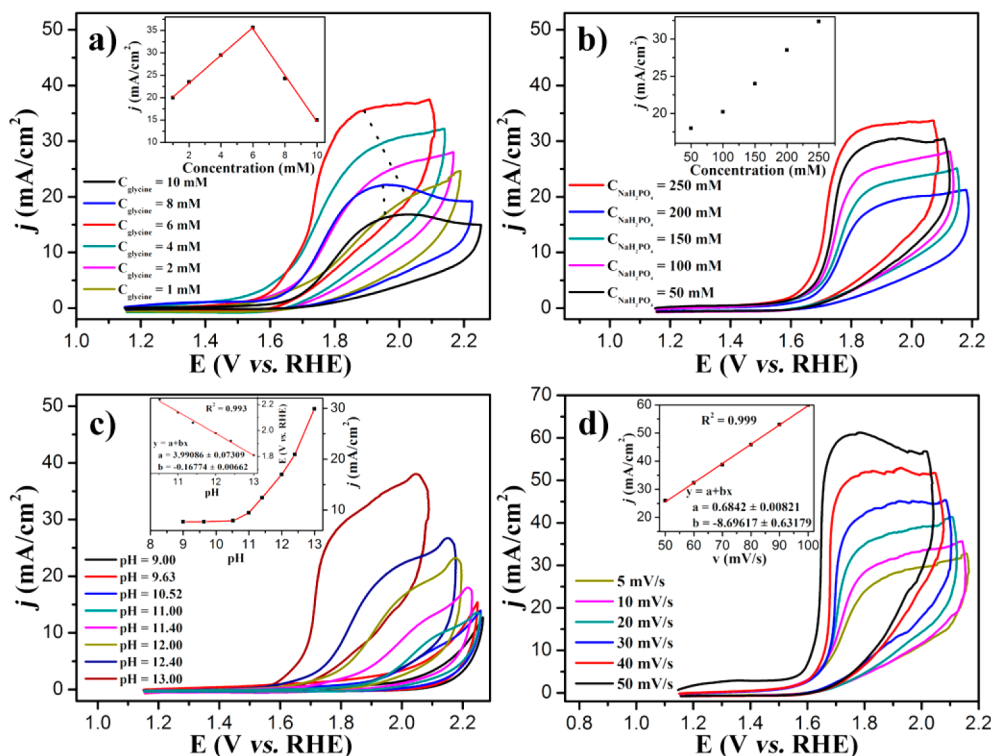


Figure 5. (a) CV features of Cu₂S NPs with different Gly concentrations in 250 mM phosphate buffer (pH = 13). Inset: Dependence of the peak current densities of Cu₂S NPs in 250 mM phosphate buffer with different concentrations of Gly. (b) CV changes of Cu₂S NPs with 6 mM Gly (pH = 13) in different concentrations of phosphate. Inset: Dependence of the peak current densities of Cu₂S NPs with 6 mM Gly in different concentrations of phosphate. (c) CV features of Cu₂S NPs with 6 mM Gly in 250 mM phosphate buffer with different pH values. Inset: Dependence of the peak current densities and potentials with different pH values. Parts a–c were carried out with a scan rate of 10 mV/s. (d) CV curves for Cu₂S NPs with 6 mM Gly in 250 mM phosphate buffer at pH = 13 with different scan rates. Inset: Linear relationship between the peak current densities and scan rates. All measurements were carried out with RDE (loading ~0.2 mg/cm²) for recording CV curves at a rotation rate of 1600 rpm.

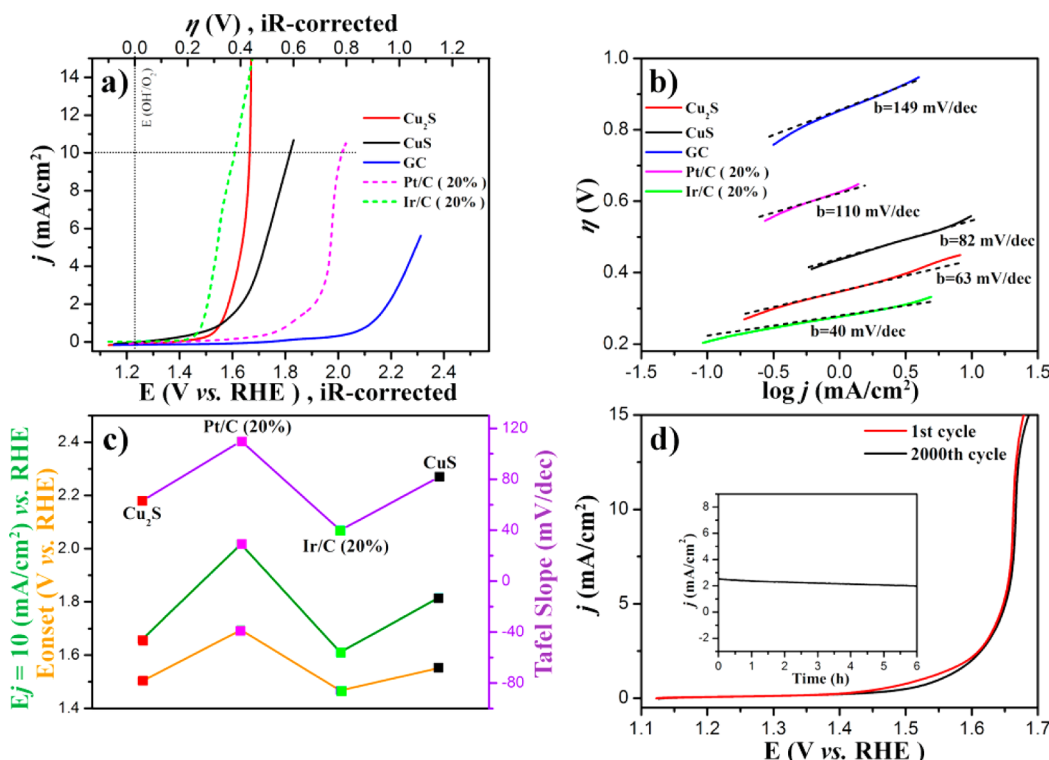


Figure 6. (a) LSV of Cu_2S , CuS , Ir/C , Pt/C , and GC electrode. LSV was measured with 6 mM Gly in 250 mM phosphate buffer (pH = 13) with a scan rate of 10 mV/s. The measurements were carried out with RDE (loading $\sim 0.2 \text{ mg}/\text{cm}^2$) for recording CV curves at a rotation rate of 1600 rpm. (b) Tafel plots ($\log j - \eta$) of Cu_2S , CuS , Ir/C , Pt/C , and GC electrode. (c) Comparison of the Tafel slopes, onset potentials, and potentials required to reach $j = 10 \text{ mA}/\text{cm}^2$ for Cu_2S , CuS , Ir/C , Pt/C , and GC electrode catalysts. (d) LSV for Cu_2S with Gly before and after 2000 CV cycles between 1.16 and 2.36 V at a scan rate of 250 mV/s. Inset: Chronoamperometric measurements for Cu_2S at a fixed applied potential of 1.83 V (vs RHE) for 6 h.

from ~ 2.16 to ~ 1.81 V (vs RHE) when the pH was increased from 9 to 13 (Figure 5c). The pH-dependent plot for the three independent measurements has a slope of -0.16774 ± 0.00662 V per pH (inset of Figure 5c). To investigate the charge-transport characteristics of Cu_2S , we recorded CV curves of the Cu_2S electrodes in 250 mM phosphate buffer (pH = 13) at various scan rates between 1.16 and 2.36 V (vs RHE; Figure 5d). With increasing scan rates, the reduction potentials show a linear relationship with the scan rates (correlation coefficient of 0.999; inset of Figure 5d), indicating that the reduction process of the prepared Cu_2S is surface-confined.⁴⁰

Then, the electrochemical activity of this new Cu_2S NP was evaluated based on the above-optimized conditions for the OER performance with 6 mM Gly in 250 mM phosphate buffer at pH = 13. For linear sweep voltammetry (LSV) and CV curves of studied materials, the ohmic potential drop (iR)⁴¹ losses arising from solution resistance were corrected (Figure S6 in the SI). Figure 6a shows LSV curves in 250 mM phosphate buffer with 6 mM Gly at pH = 13 with a scan rate of 10 mV/s. In contrast, Cu_2S with Gly exhibits considerably enhanced OER activity with an onset potential of 1.502 V slightly higher than that of Ir/C (1.467 V), and a sharp rise of the anodic current resulting from a further positive potential suggests its highly electrocatalytic activity toward OER. In addition, the overpotential of Cu_2S measured at 10 mA/cm^2 in Gly is 428 mV, which is lower than those of CuS (586 mV) and Pt/C (787 mV) and close to that of Ir/C (381 mV). At 1.658 V, the current density of Cu_2S in Gly (10 mA/cm^2) could attain 72% of the current density of Ir/C . Compared to the behavior of most nonmetals^{42–44} and even some metal catalysts like N-

doped graphene– NiCo_2O_4 ,⁴⁵ 3D NF/PC/AN,⁴⁶ mesoporous Co_3O_4 ,^{47,48} and $\text{Co}_3\text{O}_4/\text{SWNTs}$ ⁴⁹ in alkaline electrolytes (listed in Table S3 in the SI), this overpotential is favorable. Furthermore, the OER kinetics of the above catalysts were probed by corresponding Tafel plots ($\log j - \eta$); more favorable kinetics and superior catalytic activity can be seen from the much lower Tafel slope. As shown in Figure 6b, the resulting Tafel slopes are found to be ~ 63 , ~ 82 , ~ 40 , and ~ 110 mV/dec for Cu_2S , CuS , Ir/C , and Pt/C , respectively (Figure 6b,c and Table 4). Note that the Tafel slope for Cu_2S is smaller than those for CuS and Pt/C and close to that for Ir/C . Figure S7 in the SI shows an optical photograph of the Cu_2S NPs on the GC electrode during CV scans, indicating the production of many O_2 bubbles on the electrode surface.

Table 4. OER Activity Data for Different Catalysts (20% Loading) in Gly

catalyst	onset potential [V vs RHE]	η at $J = 10 \text{ mA}/\text{cm}^2$ [mV]	mass activity at $\eta = 440 \text{ mV}$ [A/g]	Tafel slope [mV/dec]	TOF ^a at $\eta = 440 \text{ mV}$ [s^{-1}]
$\text{Cu}_2\text{S/C}$	1.502	428	351.63	63	0.02916
CuS/C	1.552	586	75.48	82	0.00375
Ir/C	1.467	381	375.86	40	0.03744
Pt/C	1.695	787	9.95	110	0.00101

^aThe TOF values were obtained by assuming that every metal atom is involved in catalysis (see the Experimental Section for the calculated method).

The stability of the catalysts is always an essential aspect in their property evaluation because durability is crucial for long-term utilization. Durability studies of Cu₂S with chronoamperometric measurements were conducted in 250 mM phosphate buffer with 6 mM Gly at pH = 13 (Figure 6d). After continuous CV scanning, a negligible difference between the curves measured at the initial cycle and after 2000 CV cycles can be seen, indicating the excellent durability of Cu₂S NPs in Gly for the OER performance. When the potential was fixed at 1.83 V (vs RHE), the catalytic conditions remain stable for 6 h, remaining at 82% of the maximum value (inset of Figure 6d). Meanwhile, after the stability test, there are no obvious changes of Cu₂S NPs from the XRD and XPS results (Figures S8 and S9 in the SI), which proves that the Cu₂S NPs with Gly are stable for OER and efficiently attached to the Ketjen carbon support.

To further evaluate their OER catalytic ability, the mass activity and turnover frequency (TOF) of the above catalysts at η of 440 mV were also presented (Table 4). The calculated mass activity for Cu₂S NPs with Gly is 351.63 A/g, outperforming the other studied catalyst, CuS. The constructed Cu₂S with Gly exhibits a high TOF of 0.02916 s⁻¹, which is close to that of Ir/C (0.03744 s⁻¹), implying that the metal atom on the crystal surface was catalytically active.⁵⁰ The faradaic efficiency (FE) of Cu₂S with Gly for OER was obtained by comparing the amount of measured O₂ generated by control potential electrolysis (CPE) at 2.06 V (vs RHE) with the theoretical calculated O₂ amount. The amount of O₂ was determined by gas chromatography, and the FE was calculated to be (89.6 ± 5)% based on the total charge passing through (Figure S10 in the SI), showing that Cu₂S with 6 mM Gly serves as an effective catalyst for water oxidation, meaning that the current density is directly associated with O₂ generation but not oxidation of Gly.

It is well-accepted that the valence states of Cu cations are crucial to OER.^{12c,51} The valence state conversion of Cu cations can enhance the electrophilicity of adsorbed O, which is favorable to the formation of hydroperoxy (−OOH) species and the subsequent evolution of O₂.^{12c,51} as illustrated in Scheme 1. For Cu₂S NPs, the surface Cu^I cations, which were verified by the binding energy of Cu 2p_{3/2} at 932.3 eV (Figure 2b), should be responsible for the observed OER activity. In terms of the d-band theory, the catalytic activity of a material is dependent upon the metal d states near the Fermi level.^{4a} With respect to Cu₂S, the interaction between O₂ and the d state of the Cu atom can be considered to be the reason for the OER activity. As stated by Suntivich and co-workers,⁵ the e_g orbital of transition-metal ions take part in σ bonding with a surface-anion adsorbate, and the d-electron filling in e_g bands finally changes the bond strength of O₂-related intermediate species on the catalytic surface; these processes are important for OER.³ The great enhancement of the OER performance of Cu₂S NPs caused by Gly suggests that the aforementioned processes are considerably affected by the addition of Gly.

CONCLUSIONS

In this work, we have successfully synthesized platelet-shaped chalcocite Cu₂S NPs by a phase transformation procedure. Subsequently, the OER ability of Cu₂S was further explored by considering the effects of amino acids and some small molecules as additives. Through careful optimization of the conditions for Cu₂S with Gly for the best OER performance, we demonstrated that the addition of Gly can enhance the OER properties of Cu₂S NPs, showing a small overpotential of

428 mV at a current density of 10 mA/cm². Cu₂S NPs in a Gly solution exhibit excellent OER activity and durability, which is similar to that of the best known commercial Ir/C nanocatalysts. This phase transformation synthesis technique and Gly-assisted OER enhancement could provide new insight into the future development of highly active OER electrocatalysts.

EXPERIMENTAL SECTION

Chemicals and Materials. Copper(I) chloride (99%), oleic acid (OAc, 90%), 1-octadecene (ODE, 90%), 1-hexadecylamine (HDA, 90%), and Nafion (5 wt %) were purchased from Sigma-Aldrich. Carbon black (Ketjen EC-600J) was obtained from Akzo. Sulfur sublimed (99.5%), chloroform (99.9%), ethanol (99.9%), and hexane (99.9%) were purchased from Aladdin. For preparation of the solution, deionized water was obtained from a Millipore Autopure system (18.2 MΩ, Millipore Ltd., USA). 250 mM phosphate buffer was made by sodium dihydrogen phosphate and employed as a supporting electrolyte in the electrochemical experiment. All of the other chemicals and reagents with analytical grade were used for electrochemical measurements.

Characterization. Powder XRD patterns were collected on a Rigaku D/Max-2400 diffractometer with Cu K α radiation (λ = 1.54178 Å). TEM images were recorded on a Tecnai G2 F30 field-emission transmission electron microscope. X-ray photoelectron spectroscopy (XPS) spectra were obtained on a PHI-5702 multifunctional spectrometer using Al K α radiation.

Electrocatalytic Research. Electrochemical measurements were carried out at room temperature using a RDE made of glassy carbon (GC; RDE-3A, 3 mm diameter, 0.071 cm²) connected to a CHI 760 e Electrochemical Workstation (CHI Instruments, Shanghai Chenhua Instrument Corp., China) in a conventional three-electrode system at a scan rate of 10 mV/s with a rotation rate of 1600 rpm. Saturated Ag/AgCl (in a saturated KCl solution) was employed as a reference electrode, and a Pt net was employed as an auxiliary electrode. In this work, all electrochemical experiments were carried out at 20 ± 0.2 °C. Prior to the experiments, the GC electrode was polished with 0.3 and 0.05 μm Al₂O₃ slurry for 60 s each to obtain a mirror surface, followed by sonication in distilled water for ~60 s to remove debris, and was thoroughly rinsed with Milli-Q ultrapure water. Pt net and Ag/AgCl electrodes were used as counter and reference electrodes, respectively. The potentials were referenced to the RHE through RHE calibration,^{1b} and with 6 mM Gly in 250 mM phosphate buffer (pH = 13), $E_{\text{RHE}} = E_{\text{Ag/AgCl}} + 0.96$ V. Potentials are reported versus the Ag/AgCl reference electrode, and overpotentials (η) are calculated based on the formula $\eta = E_{\text{Ag/AgCl}} + 0.196$ V + 0.0591pH – 1.23 V.

The working electrodes were prepared according to the following methods. Briefly, 2 mg of catalyst powder was dispersed in 0.97 mL of a DMF solution with 30 μL of a Nafion solution (5 wt %, Sigma-Aldrich). The mixture was sonicated for about 1 h to generate a homogeneous ink. Then, 7 μL of the dispersion was transferred onto the GC disk, yielding a catalyst loading of ~0.2 mg/cm². The catalyst prepared was dried at room temperature; meanwhile, a polished and cleaned GC electrode as a reference was also dried for electrochemical measurement. Before the electrochemical measurement, the electrolyte (250 mM phosphate buffer, pH = 13) was purged by O₂ for 0.5 h to ensure saturation of the electrolyte. The CV curves were obtained by sweeping the potential from 1.16 to 2.36 V (vs RHE) at room temperature.

Preparation of the Sulfur Precursor Solution. Sulfur in ODE, prepared by dissolving elemental S in ODE, is used for the synthesis of metal sulfide NCs. Sulfur sublimed (3.2 mmol) was dissolved under an Ar atmosphere at 110 °C in 5 mL of ODE.

Synthesis of CuS NPs. Copper(I) chloride (0.50 mmol) and HDA (5 mmol) were dissolved in 10 mL of ODE. The solution was heated to 110 °C under a N₂ flow and kept at this temperature for 1 h to remove H₂O and other low-boiling-point impurities. Then, the sulfur in ODE (4 mL, 3 mM) was rapidly injected into the reaction flask through a syringe at 90 °C. The solution was allowed to react for 5 min, and afterward, it was quickly cooled to 70 °C. OAc were added to

the mixture at 70 °C to replace the weakly bound HDA during the cooling process. The crude solution was isolated by centrifugation and kept in chloroform for further fabrication.

Synthesis of Cu₂S NPs. A total of 2 mL of ODE and 5 mL of OAm were added to the freshly prepared CuS NPs. The solution was heated to 110 °C to remove H₂O and O₂ with vigorous magnetic stirring under a N₂ flow for 1 h in a temperature-controlled mantle. The system was heated to 220 °C at a rate of 2 °C/min, kept stirring at 220 °C for 1 h, and then cooled to room temperature. The Cu₂S NPs precipitates were collected by centrifugation at 6000 rpm and then washed by a mixture of chloroform and ethanol several times to remove precursors and surfactant residuals.

Mass Activity, TOF, and FE Calculated in Terms of the Methods Proposed by Gao and Co-workers.⁵⁰ The mass activity (A/g) values were calculated from the catalyst loading *m* (0.2 mg/cm²) and the measured current density *j* (mA/cm²) at $\eta = 440$ mV:

$$\text{mass activity} = j/m \quad (1)$$

The TOF values were calculated by assuming that every metal atom is involved in the catalysis (lower TOF limits were calculated):

$$\text{TOF} = jS/4Fn \quad (2)$$

where *j* (mA/cm²) is the measured current density at $\eta = 440$ mV, *S* (0.071 cm²) is the surface area of the GC disk, the number 4 means 4 electrons/mol of O₂, *F* is Faraday's constant (96485.3 C/mol), and *n* is the moles of coated metal atom on the electrode calculated from *m*, the molecular weight of the coated catalysts.

The FE is calculated as follows:

$$\text{FE} = n/(Q/4F) \quad (3)$$

where *n* is the moles of O₂ determined by gas chromatography, *Q* is the total charge passing through the three-electrode system, and *F* is Faraday's constant.

ASSOCIATED CONTENT

Supporting Information

Near-IR absorption spectra of the CuS and Cu₂S NPs in chloroform, oxide and reduction CV of CuS and Cu₂S NPs, structures of CuS NPs, Cu₂S NPs, and amino acids, optical photograph for the generation of O₂ bubbles on Cu₂S NP modified GC electrode, XRD pattern and XPS spectra of Cu₂S before and after stability measurements, position of the S 2p_{3/2} component for the sulfide and disulfide doublets in the CuS and Cu₂S NPs, the current density and potential values of Cu₂S with the addition of small molecules, and normalized gas chromatogram traces from a representative CPE in the presence and absence of Gly. This material is available free of charge via the Internet at <http://pubs.acs.org>.

AUTHOR INFORMATION

Corresponding Author

*E-mail: xipx@lzu.edu.cn

Notes

The authors declare no competing financial interest.

ACKNOWLEDGMENTS

We acknowledge support from the National Natural Science Foundation of China (Grants 21201092, 21403097, and 21401091), National Fund for Talent Training in Basic Science of China (No. J1103307), the Research Fund for the Doctoral Program of Higher Education (Grant 20120211120020), and the Fundamental Research Funds for the Central Universities (Lzujbky-2014-m02, Lzujbky-2014-190, and Lzujbky-2014-182). Prof. Y. Du is thankful for financial support for start-up

funding from Xi'an Jiaotong University and the National Natural Science Foundation of China (Grant 21371140).

REFERENCES

- (1) (a) Kudo, A.; Miseki, Y. *Chem. Soc. Rev.* **2009**, *38*, 253–278.
- (b) Gao, M.; Sheng, W.; Zhuang, Z.; Fang, Q.; Gu, S.; Jiang, J.; Yan, Y. *J. Am. Chem. Soc.* **2014**, *136*, 7077–7084.
- (2) Lu, Y. C.; Xu, Z. C.; Gasteiger, H. A.; Chen, S.; Hamad-Schifferli, K.; Shao-Horn, Y. *J. Am. Chem. Soc.* **2010**, *132*, 12170–12171.
- (3) (a) Cheng, F. Y.; Chen, J. *Chem. Soc. Rev.* **2012**, *41*, 2172–2192.
- (b) Liang, Y. Y.; Li, Y. G.; Wang, H. L.; Dai, H. J. *J. Am. Chem. Soc.* **2013**, *135*, 2013–2036. (c) Wang, H.; Dai, H. *Chem. Soc. Rev.* **2013**, *42*, 3088–3113.
- (4) (a) Matsumoto, Y.; Sato, E. *Mater. Chem. Phys.* **1986**, *14*, 397–426. (b) Walter, M. G.; Warren, E. L.; McKone, J. R.; Boettcher, S. W.; Mi, Q.; Santori, E. A.; Lewis, N. S. *Chem. Rev.* **2010**, *110*, 6446–6473.
- (c) Trasatti, S. In *Interfacial Electrochemistry*; Wieckowski, A., Ed.; Marcel Dekker, Inc.: New York, 1999; pp 769–792.
- (5) Suntivich, J.; May, K. J.; Gasteiger, H. A.; Goodenough, J. B.; Shao-Horn, Y. *Science* **2011**, *334*, 1383–1385.
- (6) Lee, S. W.; Carlton, C.; Risch, M.; Surendranath, Y.; Chen, S.; Furutsuki, S.; Yamada, A.; Nocera, D. G.; Shao-Horn, Y. *J. Am. Chem. Soc.* **2012**, *134*, 16959–16962.
- (7) Mirzakulova, E.; Khatmullin, R.; Walpita, J.; Corrigan, T.; Vargas-Barbosa, N. M.; Vyas, S.; Oottikkal, S.; Manzer, S. F.; Hadad, C. M.; Glusac, K. D. *Nat. Chem.* **2010**, *4*, 794–801.
- (8) Dau, H.; Limberg, C.; Reier, T.; Risch, M.; Roggan, S.; Strasser, P. *ChemCatChem* **2010**, *2*, 724–761.
- (9) (a) Eisenberg, R.; Gray, H. B. *Inorg. Chem.* **2008**, *47*, 1697–1699.
- (b) Barber, J. *Chem. Soc. Rev.* **2009**, *38*, 185–196.
- (10) Chen, S.; Duan, J. J.; Jaroniec, M.; Qiao, S.-Z. *Adv. Mater.* **2014**, *26*, 2925–2930.
- (11) Gorlin, Y.; Jaramillo, T. F. *J. Am. Chem. Soc.* **2010**, *132*, 13612–13614.
- (12) (a) Gorlin, Y.; Jaramillo, T. F. *J. Am. Chem. Soc.* **2010**, *132*, 13612–13614. (b) Liang, Y. Y.; Li, Y. G.; Wang, H. L.; Zhou, J. G.; Wang, J.; Regier, T.; Dai, H. J. *Nat. Mater.* **2011**, *10*, 780–786.
- (c) Yeo, B. S.; Bell, A. T. *J. Am. Chem. Soc.* **2011**, *133*, 5587–5593.
- (13) (a) Li, Y. G.; Hasin, P.; Wu, Y. Y. *Adv. Mater.* **2010**, *22*, 1926–1929. (b) Gong, M.; Li, Y. G.; Wang, H. L.; Liang, Y. Y.; Wu, J. Z.; Zhou, J. G.; Wang, J.; Regier, T.; Wei, F.; Dai, H. J. *J. Am. Chem. Soc.* **2013**, *135*, 8452–8455. (c) Chen, S.; Qiao, S. Z. *ACS Nano* **2013**, *7*, 10190–10196. (d) Chen, S.; Duan, J. J.; Jaroniec, M.; Qiao, S. Z. *Angew. Chem., Int. Ed.* **2013**, *52*, 13567–13570.
- (14) (a) Gao, M. R.; Xu, Y. F.; Jiang, J.; Zheng, Y. R.; Yu, S. H. *J. Am. Chem. Soc.* **2012**, *134*, 2930–2933. (b) Gao, M. R.; Xu, Y. F.; Jiang, J.; Yu, S. H. *Chem. Soc. Rev.* **2013**, *42*, 2986–3017.
- (15) (a) Kanan, M. W.; Nocera, D. G. *Science* **2008**, *321*, 1072–1075.
- (b) Cobo, S.; Heidkamp, J.; Jacques, P. A.; Fize, J.; Fourmond, V.; Guetaz, L.; Jousselleme, B.; Ivanova, V.; Dau, H.; Palacin, S.; Fontecave, M.; Artero, V. *Nat. Mater.* **2012**, *11*, 802–807.
- (16) Dinca, M.; Surendranath, Y.; Nocera, D. G. *Proc. Natl. Acad. Sci. U.S.A.* **2010**, *107*, 10337–10341.
- (17) May, K. J.; Carlton, C. E.; Stoerzinger, K. A.; Risch, M.; Suntivich, J.; Lee, Y. L.; Grimaud, A.; Shao-Horn, Y. *J. Phys. Chem. Lett.* **2012**, *3*, 3264–3270.
- (18) Yin, Q. S.; Tan, J. M.; Besson, C.; Geletii, Y. V.; Musaev, D. G.; Kuznetsov, A. E.; Luo, Z.; Hardcastle, K. I.; Hill, C. L. *Science* **2010**, *328*, 342–345.
- (19) Suntivich, J.; May, K. J. H.; Gasteiger, A.; Goodenough, J. B.; Shao-Horn, Y. *Science* **2011**, *334*, 1383–1385.
- (20) Barnett, S. M.; Goldberg, K. I.; Mayer, J. M. *Nat. Chem.* **2012**, *4*, 498–502.
- (21) Chen, Z.; Meyer, T. J. *Angew. Chem., Int. Ed.* **2013**, *52*, 700–703.
- (22) Zhang, M.-T.; Chen, Z.; Kang, P.; Meyer, T. J. *J. Am. Chem. Soc.* **2013**, *135*, 2048–2051.
- (23) Pita, M.; Mate, D. M.; Gonzalez-Perez, D.; Shleev, S.; Fernandez, V. M.; Alcalde, M.; De Lacey, A. L. *J. Am. Chem. Soc.* **2014**, *136*, 5892–5895.

- (24) Liu, G.; Schulmeyer, T.; Brötz, J.; Klein, A.; Jaegermann, W. *Thin Solid Films* **2003**, *431*, 477–482.
- (25) Sakamoto, T.; Sunamura, H.; Kawaura, H.; Hasegawa, T.; Nakayama, T.; Aono, M. *Appl. Phys. Lett.* **2003**, *82*, 3032–3034.
- (26) Wang, D.; Ghirlanda, G.; Allen, J. P. *J. Am. Chem. Soc.* **2014**, *136*, 10198–10201.
- (27) (a) An, L.; Huang, L.; Liu, H.; Xi, P.; Chen, F.; Du, Y. *Part. Part. Syst. Charact.* **2015**, DOI: 10.1002/ppsc.201400209. (b) Du, W.; Qian, X.; Ma, X.; Gong, Q.; Cao, H.; Yin, J. *Chem.—Eur. J.* **2007**, *13*, 3241–3247.
- (28) Xie, Y.; Riedinger, A.; Prato, M.; Casu, A.; Genovese, A.; Guardia, P.; Sottini, S.; Sangregorio, C.; Miszta, K.; Ghosh, S.; Pellegrino, T.; Manna, L. *J. Am. Chem. Soc.* **2013**, *135*, 17630–17637.
- (29) (a) Bard, A. J.; Faulkner, L. R. *Electrochemical Methods: Fundamentals and Applications*; Wiley: New York, 1980; pp 1–864. (b) Li, Z.; Lui, A. L. K.; Lam, K. H.; Xi, L.; Lam, Y. M. *Inorg. Chem.* **2014**, *53*, 10874–10880.
- (30) (a) Li, X.; Shen, H.; Li, S.; Niu, J. Z.; Wang, H.; Li, L. S. *J. Mater. Chem.* **2010**, *20*, 923–928. (b) Su, Y.; Lu, X.; Xie, M.; Geng, H.; Wei, H.; Yang, Z.; Zhang, Y. *Nanoscale* **2013**, *5*, 8889–8893.
- (31) Martinson, A. B. F.; Riha, S. C.; Thimsen, E.; Elam, J. W.; Pellin, M. J. *Energy Environ. Sci.* **2013**, *6*, 1868–1878.
- (32) Wang, Y.; Ai, X.; Miller, D.; Rice, P.; Topuria, T.; Krupp, L.; Kellock, A.; Song, Q. *CrystEngComm* **2012**, *4*, 7560–7562.
- (33) Okada, Y.; Ohtani, T.; Yokota, Y.; Tachibana, Y.; Morishige, K. *J. Electron Microsc.* **2000**, *49*, 25–29.
- (34) Skomorokhov, A. N.; Trots, D. M.; Knapp, M.; Bickulova, N. N.; Fuess, H. *J. Alloys Compd.* **2006**, *421*, 64–71.
- (35) (a) Liu, H.; Shi, X.; Xu, F.; Zhang, L.; Zhang, W.; Chen, L.; Li, Q.; Uher, C.; Day, T.; Snyder, G. J. *Nat. Mater.* **2012**, *11*, 422–425. (b) Wu, X.-J.; Huang, X.; Liu, J.; Yang, J.; Li, B.; Huang, W.; Zhang, H. *Angew. Chem., Int. Ed.* **2014**, *53*, 5083–5087. (c) Takahashi, T.; Yamamoto, O.; Matsuyama, F.; Noda, Y. *J. Solid. State Chem.* **1976**, *16*, 35–39.
- (36) (a) O’Neil, R. D.; Chang, S.; Lowry, J. P.; McNeil, C. J. *Biosens. Bioelectron.* **2004**, *19*, 1521–1528. (b) Sun, X.; Guo, S.; Liu, Y.; Sun, S. *Nano Lett.* **2012**, *12*, 4859–4863.
- (37) Kwapien, K.; Piccinin, S.; Fabris, S. *J. Phys. Chem. Lett.* **2013**, *4*, 4223–4230.
- (38) (a) Kim, M. K.; Martell, A. E. *J. Am. Chem. Soc.* **1966**, *88*, 914–918. (b) Nagy, N. V.; Szabo-Planka, T.; Rockenbauer, A.; Peintler, G.; Nagypal, I.; Korecz, L. *J. Am. Chem. Soc.* **2003**, *125*, 5227–5235.
- (39) Wang, D.; Ghirlanda, G.; Allen, J. P. *J. Am. Chem. Soc.* **2014**, *136*, 10198–10201.
- (40) Bai, J.; Jiang, X. *Anal. Chem.* **2013**, *85*, 8095–8101.
- (41) Wang, L.; Lin, C.; Huang, D.; Zhang, F.; Wang, M.; Jin, J. *ACS Appl. Mater. Interfaces* **2014**, *6*, 10172–10180.
- (42) Park, H. W.; Lee, D. U.; Liu, Y.; Wu, J.; Nazar, L. F.; Chen, Z. J. *Electrochem. Soc.* **2013**, *160*, A2244–A2250.
- (43) Chen, S.; Duan, J.; Jaroniec, M.; Qiao, S. *Adv. Mater.* **2014**, *26*, 2925–2930.
- (44) Tian, J.; Liu, Q.; Asiri, A. M.; Alamry, K. A.; Sun, X. *ChemSusChem* **2014**, *7*, 2125–2130.
- (45) Chen, S.; Qiao, S. *ACS Nano* **2013**, *7*, 10190–10196.
- (46) Wang, J.; Zhang, H.; Qin, Y.; Zhang, X. *Angew. Chem., Int. Ed.* **2013**, *52*, 5248–5253.
- (47) Grewe, T.; Deng, X.; Weidenthaler, C.; Schüth, F.; Tüysüz, H. *Chem. Mater.* **2013**, *25*, 4926–4935.
- (48) Tüysüz, H.; Hwang, Y. J.; Khan, S. B.; Asiri, A. M.; Yang, P. *Nano Res.* **2013**, *6*, 47–54.
- (49) Wu, J.; Xue, Y.; Yan, X.; Yan, W.; Cheng, Q.; Xie, Y. *Nano Res.* **2012**, *5*, 521–530.
- (50) Gao, M.-R.; Cao, X.; Gao, Q.; Xu, Y.-F.; Zheng, Y.-R.; Jiang, J.; Yu, S.-H. *ACS Nano* **2014**, *8*, 3970–3978.
- (51) Chou, N. H.; Ross, P. N.; Bell, A. T.; Tilley, T. D. *ChemSusChem* **2011**, *4*, 1566–1569.